THE JOURNAL OF PHYSICAL CHEMISTRY LETTERS
A JOURNAL OF THE AMERICAN CHEMICAL SOCIETY

pubs.acs.org/JPCL

Letter

Molecular Concentration Determination Using Long-Interval Chemical Exchange Inversion Transfer (CEIT) NMR Spectroscopy

Weiping Jiang,[‖] Qianni Guo,[‖] Qing Luo, Xiaoxiao Zhang, Yaping Yuan, Haidong Li, and Xin Zhou*

Cite This: *J. Phys. Chem. Lett.* 2021, 12, 8652−8657

Read Online

ACCESS | Metrics & More | Article Recommendations | Supporting Information

ABSTRACT: Functionalized hyperpolarized xenon "cage" molecules have often been used for ultrasensitive detection of biomolecules and microenvironment properties. However, the rapid and accurate measurement of molecule concentration is still a challenge. Here, we report a molecule concentration measurement method using long-interval chemical exchange inversion transfer (CEIT) NMR spectroscopy. The molecule concentration can be quantitatively measured with only 2 scans, which shortens the acquisition time by about 10 times compared to conventional Hyper-CEST (chemical exchange saturation transfer) z-spectrum method. Moreover, we found that the accuracy of concentration determination would be the best when the CEIT effect is $1-1/e$ or close to it, and a relative deviation of CrA-$(COOH)_6$ less than ±1% has been achieved by only a one-step optimization of the number of cycles. The proposed method enables efficient and accurate determination of molecule concentration, which provides a potential way for rapid quantitative molecular imaging applications.

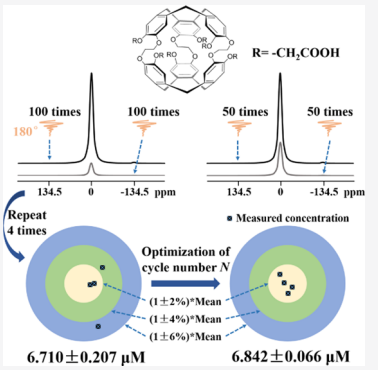

The quantitative measurement of analytes at ultralow concentrations plays a crucial role in chemistry and many applied fields. Optical and electrochemical analysis methods have been frequently used for the quantitative measurement of concentration.[1,2] However, the poor penetration depth or invasiveness has limited their applications in living and other opaque systems. As a penetration depth-unlimited and noninvasive analytical tool, nuclear magnetic resonance (NMR) spectroscopy has been exploited for concentration quantification. However, the intrinsically low sensitivity of conventional NMR limits its application in the measurement of analytes with ultralow concentrations. Hyper-CEST,[3] which combines the advantages of both chemical exchange saturation transfer (CEST)[4] and spin exchange optical pumping (SEOP)[5] techniques, has shown picomole and subpicomole level's detection sensitivity by groups.[6−8] Hyperpolarized xenon has been used for the detection of biomacromolecules (such as proteins,[9−11] enzymes,[12−14] nucleic acids,[15] and transmembrane receptor targets[16−19]), metabolites (biothiol,[20,21] ribose,[22] maltose,[23] and H_2S[24]), microenvironment properties (pH[7,25] and temperature[26−28]), and metal ions (zinc,[29,30] mercury,[31] and lead and cadmium[32]) with specifically designed xenon-host molecules.[22,23,33,34] The determination of xenon-host molecule concentrations will enable a better understanding of chemical or biological processes.

An analytical solution for hyperpolarized nuclei has been derived from the Bloch−McConnell equations.[35] The exchange dynamic parameters have been quantitatively evaluated using different methods.[36−38] The xenon-host molecule binding parameters and exchange rate could be fitted using the z-spectra obtained at different B_1 levels using the full Hyper-CEST solution method.[39−41] A model has been proposed to measure the unknown host molecule concentration by fitting with the CEST effect and free xenon depletion rate.[42] With the model for data analysis, a host molecule concentration was quantitatively measured in the nanomole range. Despite the substantial sensitivity advantage of Hyper-CEST, the acquisition time for Hyper-CEST quantification (~10 min for an entire z-spectrum) was typically long due to the hyperpolarized xenon renewal time before each scan and the multiple scans with different parameters. The ultrafast Hyper-CEST method was proposed to accelerate data acquisition.[43] The ultrafast Hyper-CEST method was used to monitor the enzyme activity through a quantitative measurement of cucurbit[6]uril (CB6) concentration with an initial known CB6 concentration.[44] The acquisition time for concentration determination is ~30 s; however, this method encodes the free xenon signal in a certain chemical shift range, resulting in a low xenon signal-to-noise ratio which will influence the accuracy of concentration determination. Thus, methods for the rapid and accurate measurement of unknown concentrations of xenon-host molecules are still lacking.

In this work, we proposed a molecular concentration determination method using long-interval chemical exchange inversion transfer (CEIT) NMR spectroscopy. We demon-

Received: July 12, 2021
Accepted: August 26, 2021

https://doi.org/10.1021/acs.jpclett.1c02239
J. Phys. Chem. Lett. 2021, 12, 8652−8657

strated the method with CrA-$(COOH)_6$ (Figure S1), a derivative of the most widely used xenon-host molecule (cryptophane-A), as the tested molecule. We derived an analytical expression for the xenon-host molecule concentration using CEIT with the assumption of a sufficiently long interval time. Unknown CrA-$(COOH)_6$ concentrations in solution have been determined with only 2 scans using the long-interval CEIT method. The acquisition time for concentration determination is about 10 times shorter than that of the conventional Hyper-CEST method which requires acquisition of entire z-spectra. Moreover, we theoretically and experimentally demonstrated that when the CEIT effect is $1-1/e$ or close to it, the accuracy of concentration determination will be the best. Through only a one-step optimization of the number of cycles, a relative deviation less than ±1% was achieved with the measured concentration improved from 6.7 ± 0.2 μM to 6.8 ± 0.1 μM.

Figure 1 illustrates the CEIT pulse sequence consists of xenon renewal time followed by N cycles of 180° pulse-interval

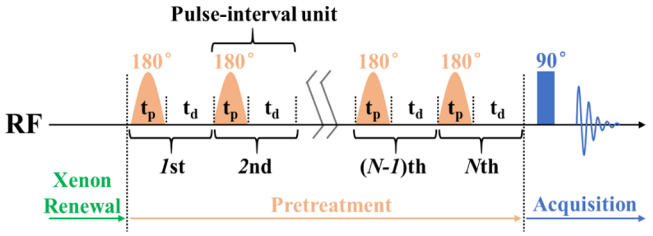

Figure 1. CEIT pulse sequence diagram. The 180° pulses are Gaussian pulse truncated at 20% with pulse length (t_p) of 4 ms, t_d is the interval time between 180° pulses, and N is the number of pulse-interval unit repeat time.

units for pretreatment before a 90° bp pulse excited for acquisition. All 180° pulses used in the study are Gaussian pulses truncated at 20% with pulse length (t_p) of 4 ms. t_d is the interval time between 180° pulses. The radio frequency (RF) duty cycle is given by $t_p/(t_p + t_d)$. The derivation of the host molecule concentration expression based on reasonable assumptions is shown in the Supporting Information (section S1). The total host molecule concentration ($[HM]$) in solution is given as

$$[HM] = \frac{1 - CEITR^{1/N}}{2}\left(\frac{1}{K} + [\mathrm{Xe}]\right) \quad (1)$$

where $CEITR$ is determined by M_{on}/M_{off}, the CEIT effect equals 1-$CEITR$, M_{on} and M_{off} stand for the magnetization of on-resonance and off-resonance experiments respectively, N is the number of cycles, K is the binding constant, and [Xe] is the free xenon concentration in solution.

To investigate the CEIT effect dependence on experimental parameters, we prepared a 2.5 μM CrA-$(COOH)_6$ solution as the tested sample. The continuous wave (CW) CEST z-spectrum (CW saturation of 12.4 s and 10.6 μT) and the CEIT z-spectrum (200 cycles and t_d = 120 ms) over the chemical shift range from 50 ppm to −195 ppm are shown in Figure 2a. Free xenon at 0 ppm and CrA-$(COOH)_6$-bound xenon at −134.5 ppm are observed. The oscillation near 0 ppm in the CEIT z-spectrum is induced by the truncation of 180° pulses, and the asymmetric amplitude near 0 ppm may be contributed to the small shift of free xenon signal and measure error (Figure S4). The oscillation is similar to a ^{1}H pulsed CEST

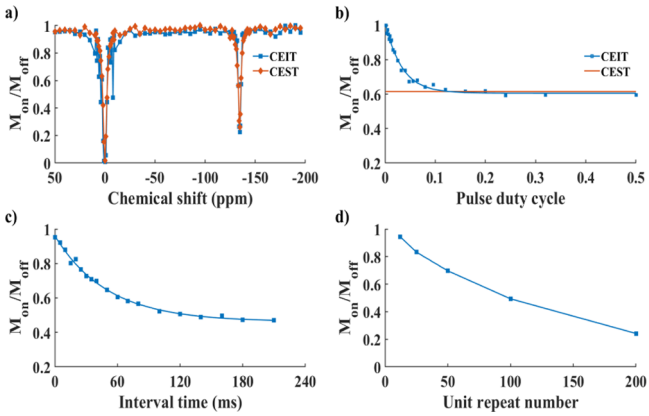

Figure 2. Characterization of CEIT. a) z-spectra achieved by CEST (CW saturation of 12.4 s and 10.6 μT, red diamonds) and CEIT (200 cycles and t_d = 120 ms, blue squares) methods. The two methods achieve two signals (free xenon at 0 ppm and CrA-$(COOH)_6$-bound xenon at −134.5 ppm). b) Comparison of the CEIT effect (blue) of different RF duty cycles ($t_p/(t_p + t_d)$) and CEST contrast (red) with total pretreatment time of 5 s. CEIT obtains similar contrast with CW CEST when the duty cycle is larger than 0.12. c) and d) are the CEIT effect as a function of interval time (fixed N = 100) and cycles (fixed t_d = 150 ms), respectively. The CEIT effect increases with both the interval time and the number of cycles.

result in a previous report.[45] Thus, a highly selective 180° pulse is needed when the chemical shift of the host-molecule-bound xenon is close to 0 ppm. Figure 2b shows the CEIT effects of different RF duty cycles (0.0016−0.5) and the CW CEST (CW saturation of 5 s and 10.6 μT) effect with the same total pretreatment time of 5 s. The CEIT effect increases with the RF duty cycle and gradually approaches the CEST effect with CW irradiation. The CEIT method obtains a similar contrast with the CW CEST when the RF duty cycles are larger than 0.12. Compared with the CW CEST, the CEIT can substantially reduce the RF energy deposition during the scan. Figure 2c shows that the $CEITR$ exponentially decreases with interval time t_d and fixed number of cycles N = 100. The CEIT effect reaches a plateau with a sufficiently long interval time, thereby showing that the inverted CrA-$(COOH)_6$-bound xenon exchanged sufficiently with free xenon. The fitted exchange rate is about 15.35 Hz (Figure S5), which agrees well with the result in previous study.[38] Unless otherwise stated, the interval time used in the later CEIT experiments was set to t_d = 150 ms. The relationship between the CEIT effect and the number of cycles is shown in Figure 2d. The CEIT effect increases with the number of cycles.

To quantitatively determine the unknown CrA-$(COOH)_6$ concentration, three CrA-$(COOH)_6$ solutions with different concentrations (S1−S3: 4.9, 7.2, and 9.3 μM) were prepared as "unknown" samples. NMR spectra (NS = 16) and CEIT z-spectra (100 cycles and t_d = 150 ms) ranging from −145 ppm to −125 ppm are shown in Figure 3a and Figure 3b, respectively. Both the CrA-$(COOH)_6$-bound xenon signal intensity in NMR spectra and the CEIT effect in z-spectra increase with the concentration. As shown in section S2 of the Supporting Information, the binding constant K of CrA-$(COOH)_6$ obtained using the relative peak integrals in the direct NMR spectroscopy is approximately 3322 M^{-1}. The free xenon concentration can be calculated using the solubility of xenon in water and the partial pressure of xenon.[46] Thus, the free xenon concentration is 4.4 mM/atm × (65.7 psi/14.696

https://doi.org/10.1021/acs.jpclett.1c02239
J. Phys. Chem. Lett. 2021, 12, 8652−8657

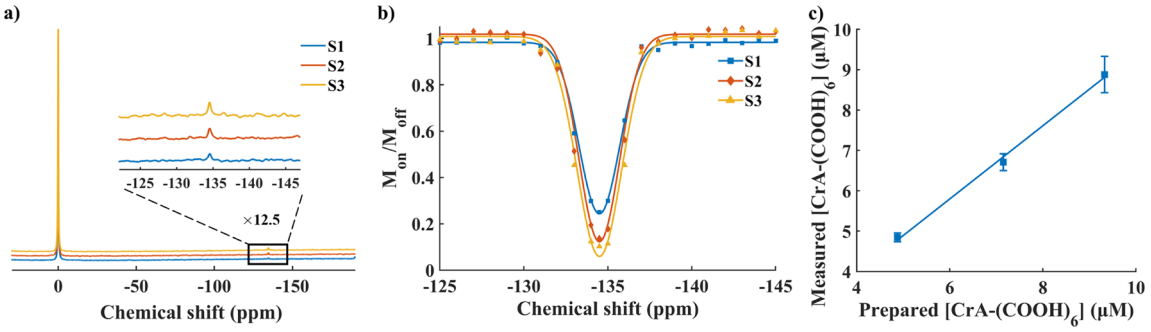

Figure 3. Concentration determination of CrA-$(COOH)_6$. The NMR spectroscopy and z-spectra of three different CrA-$(COOH)_6$ concentrations (S1, 4.9 μM, blue squares; S2, 7.2 μM, red diamonds; and S3, 9.3 μM, orange triangles) are shown in a) and b), respectively. Both the CrA-$(COOH)_6$-bound xenon signal intensity in NMR spectra and the CEIT effect in z-spectra increase with the concentration. c) The comparison of the measured CrA-$(COOH)_6$ concentrations and prepared CrA-$(COOH)_6$ concentrations. The measured CrA-$(COOH)_6$ concentrations agree well with the prepared CrA-$(COOH)_6$ concentrations ($y = 0.907x + 0.355$, $R^2 = 0.997$).

psi·atm^{-1}) × 0.02 ≈ 393.4 μM with the experimental settings. The CrA-$(COOH)_6$ concentration can be calculated using eq 1 with the measured *CEITR*. With 4 repeats, the average *CEITRs* of samples S1−S3 under 100 cycles are 0.245 ± 0.008, 0.142 ± 0.009, and 0.076 ± 0.009, individually. The measured concentrations of samples S1−S3 are 4.8 ± 0.1 μM, 6.7 ± 0.2 μM and 8.9 ± 0.5 μM, respectively. Figure 3c shows the comparison of the measured concentrations and prepared concentrations. The measured concentrations agree well with the prepared concentrations. The long-interval CEIT method can therefore quantify the CrA-$(COOH)_6$ concentration in 2 scans with prior knowledge of binding constant K and solvent condition. The total acquisition time of long-interval CEIT method is ∼76 s, which is about 10 times shorter than that of conventional Hyper-CEST quantification method (∼770 s),[39−41] which provides access to the full parameter set. The limitation here is similar to a recent work by Kunth et. al that performs quantification with one reference sample.[41] Furthermore, the concentration measurement in this work is carried out at low concentration range, in which the effect of aggregation on the concentration quantification is negligible (Figure S6, Figure S7).[47] In addition, the hyperpolarized xenon renewal time before each scan is another element contributing to the long acquisition time, which can be further reduced by improving xenon polarization level in the future.

However, the standard deviations of the measured concentrations are different from the standard deviations of the *CEITRs* for samples S1−S3 under 100 cycles. To evaluate the accuracy of the concentration measurement by the long-interval CEIT method, we conducted CEIT experiments with different numbers of cycles (12, 25, 50, 100, and 200 cycles) for samples S1−S3. The measured CEIT effects are shown in Figure S8, and the measured concentrations are shown in Figure 4. The standard deviations of the measured concentrations first decreases and then increases with the CEIT effect for all samples. Because of the low on-resonance signal intensity under 200 cycles, the measured concentrations of samples S2 and S3 are overlapped. A deviation analysis of fr (fr is the ratio between host-molecule-bound xenon and free xenon) in the Supporting Information (section S3) shows that the relative deviation reaches its minimum value when the CEIT effect is or close to $1-1/e$. To improve the accuracy of concentration determination, an optimal cycle number determined by formula (A29) in the Supporting Information is needed. For sample S2, the *CEITR* is 0.142 ± 0.009, and the

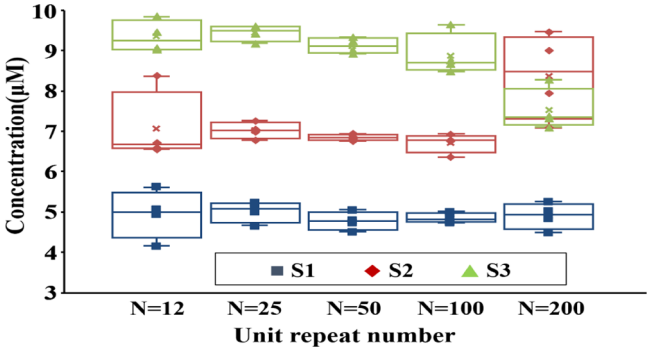

Figure 4. Concentration determination of sample S1 (blue squares), S2 (red diamonds), and S3 (green triangles) under different unit repeat numbers (N = 12, 25, 50, 100 and 200).

measured concentration is 6.7 ± 0.2 μM under 100 cycles. The optimal number of cycles is calculated to be approximately 51. When the number of cycles was set to 50, the measured *CEITR* is 0.370 ± 0.004 and the measured concentration is 6.8 ± 0.1 μM with a relative deviation less than ±1%. Thus, the long-interval CEIT method can significantly improve the accuracy of CrA-$(COOH)_6$ concentration determination with only a one-step optimization of the number of cycles. Furthermore, the unknown concentration might also be quantified by combining CEIT method with other strategies, such as the standard addition strategy.[48] Although our study investigated only the long-interval CEIT method, the results might be generalized to the pulsed Hyper-CEST and CW Hyper-CEST methods. For example, adjusting the saturation time to make the measured CEST contrast $1-1/e$ or close to it to improve the determination accuracy. In addition, the long-interval CEIT method is also compatible with signal enhancement methods, such as Hyper-SAGE[49] and Hyper-SAME[50] in the previous report, which may further improve the detection sensitivity.

In summary, we successfully demonstrated a new method for the accurate determination of molecular concentrations with a priori information. The unknown CrA-$(COOH)_6$ concentration could be quantitatively determined with only 2 scans, which makes the total acquisition time about 10 times shorter than that of conventional Hyper-CEST method. The accuracy of CrA-$(COOH)_6$ concentration determination would be the best when the CEIT effect is $1-1/e$ or close to it. A measured concentration with a relative deviation less than ±1% was

https://doi.org/10.1021/acs.jpclett.1c02239
J. Phys. Chem. Lett. 2021, 12, 8652−8657

achieved through only a one-step optimization of the number of cycles. The long-interval CEIT method makes accurate determination of molecule concentration efficient, which provides a potential way for the rapid quantitative molecular imaging applications.

■ ASSOCIATED CONTENT

Supporting Information

The Supporting Information is available free of charge at https://pubs.acs.org/doi/10.1021/acs.jpclett.1c02239.

Experimental description; derivation of xenon host molecule concentration expression; measurement of the binding constant of CrA-$(COOH)_6$; analysis of the standard deviation of concentration determination; the structure of CrA-$(COOH)_6$; the CEIT pulse sequence diagram; 2.5 μM CrA-$(COOH)_6$ ^{129}Xe NMR spectroscopy; the local CEIT z-spectra achieved with different experimental settings; the exchange rate fitting of 2.5 μM CrA-$(COOH)_6$ at 297 K and 65.7 psi; DLS data showing size distribution by number in aqueous solution at 298 K of 100.0 μM CrA-$(COOH)_6$ and 10.5 μM CrA-$(COOH)_6$; the comparison of the measured CrA-$(COOH)_6$ concentrations and prepared CrA-$(COOH)_6$ concentrations ranges from 10.5 nM to 10.5 μM; the CEIT effect of samples S1−S3 under variable unit repeat numbers (PDF)

■ AUTHOR INFORMATION

Corresponding Author

Xin Zhou − *Key Laboratory of Magnetic Resonance in Biological Systems, State Key Laboratory of Magnetic Resonance and Atomic and Molecular Physics, National Center for Magnetic Resonance in Wuhan, Wuhan Institute of Physics and Mathematics, Innovation Academy for Precision Measurement Science and Technology, Chinese Academy of Sciences-Wuhan National Laboratory for Optoelectronics, Wuhan 430071, People's Republic of China; University of Chinese Academy of Sciences, Beijing 100049, People's Republic of China;* orcid.org/0000-0002-5580-7907; Phone: +86 278 719 8802; Email: xinzhou@wipm.ac.cn

Authors

Weiping Jiang − *Key Laboratory of Magnetic Resonance in Biological Systems, State Key Laboratory of Magnetic Resonance and Atomic and Molecular Physics, National Center for Magnetic Resonance in Wuhan, Wuhan Institute of Physics and Mathematics, Innovation Academy for Precision Measurement Science and Technology, Chinese Academy of Sciences-Wuhan National Laboratory for Optoelectronics, Wuhan 430071, People's Republic of China; University of Chinese Academy of Sciences, Beijing 100049, People's Republic of China*

Qianni Guo − *Key Laboratory of Magnetic Resonance in Biological Systems, State Key Laboratory of Magnetic Resonance and Atomic and Molecular Physics, National Center for Magnetic Resonance in Wuhan, Wuhan Institute of Physics and Mathematics, Innovation Academy for Precision Measurement Science and Technology, Chinese Academy of Sciences-Wuhan National Laboratory for Optoelectronics, Wuhan 430071, People's Republic of China; University of Chinese Academy of Sciences, Beijing 100049, People's Republic of China*

Qing Luo − *Key Laboratory of Magnetic Resonance in Biological Systems, State Key Laboratory of Magnetic Resonance and Atomic and Molecular Physics, National Center for Magnetic Resonance in Wuhan, Wuhan Institute of Physics and Mathematics, Innovation Academy for Precision Measurement Science and Technology, Chinese Academy of Sciences-Wuhan National Laboratory for Optoelectronics, Wuhan 430071, People's Republic of China*

Xiaoxiao Zhang − *Key Laboratory of Magnetic Resonance in Biological Systems, State Key Laboratory of Magnetic Resonance and Atomic and Molecular Physics, National Center for Magnetic Resonance in Wuhan, Wuhan Institute of Physics and Mathematics, Innovation Academy for Precision Measurement Science and Technology, Chinese Academy of Sciences-Wuhan National Laboratory for Optoelectronics, Wuhan 430071, People's Republic of China*

Yaping Yuan − *Key Laboratory of Magnetic Resonance in Biological Systems, State Key Laboratory of Magnetic Resonance and Atomic and Molecular Physics, National Center for Magnetic Resonance in Wuhan, Wuhan Institute of Physics and Mathematics, Innovation Academy for Precision Measurement Science and Technology, Chinese Academy of Sciences-Wuhan National Laboratory for Optoelectronics, Wuhan 430071, People's Republic of China; University of Chinese Academy of Sciences, Beijing 100049, People's Republic of China*

Haidong Li − *Key Laboratory of Magnetic Resonance in Biological Systems, State Key Laboratory of Magnetic Resonance and Atomic and Molecular Physics, National Center for Magnetic Resonance in Wuhan, Wuhan Institute of Physics and Mathematics, Innovation Academy for Precision Measurement Science and Technology, Chinese Academy of Sciences-Wuhan National Laboratory for Optoelectronics, Wuhan 430071, People's Republic of China; University of Chinese Academy of Sciences, Beijing 100049, People's Republic of China*

Complete contact information is available at: https://pubs.acs.org/10.1021/acs.jpclett.1c02239

Author Contributions

[||]Weiping Jiang and Qianni Guo contributed equally to this work.

Notes

The authors declare no competing financial interest.

■ ACKNOWLEDGMENTS

This work is supported by the National Key R&D Program of China (2018YFA0704000), the National Natural Science Foundation of China (91859206, 81625011, 21921004, 81901737 and 81971705), the Key Research Program of Frontier Sciences (ZDBS-LY-JSC004), and the Scientific Instrument Developing Project (GJJSTD20200002) of the Chinese Academy of Sciences. X. Zhou acknowledges the support from the Tencent Foundation through the XPLORER PRIZE.

■ REFERENCES

(1) Yue, Y.; Huo, F.; Ning, P.; Zhang, Y.; Chao, J.; Meng, X.; Yin, C. Dual-Site Fluorescent Probe for Visualizing the Metabolism of Cys in Living Cells. *J. Am. Chem. Soc.* **2017**, *139* (8), 3181−3185.

(2) Liu, J.; Cao, Z.; Lu, Y. Functional Nucleic Acid Sensors. *Chem. Rev.* **2009**, *109* (5), 1948−98.

(3) Schröder, L.; Lowery, T. J.; Hilty, C.; Wemmer, D. E.; Pines, A. Molecular Imaging Using a Targeted Magnetic Resonance Hyperpolarized Biosensor. *Science* **2006**, *314* (5798), 446−449.
(4) Ward, K. M.; Aletras, A. H.; Balaban, R. S. A New Class of Contrast Agents for MRI Based on Proton Chemical Exchange Dependent Saturation Transfer (CEST). *J. Magn. Reson.* **2000**, *143* (1), 79−87.
(5) Li, H.; Zhang, Z.; Zhong, J.; Ruan, W.; Han, Y.; Sun, X.; Ye, C.; Zhou, X. Oxygen-Dependent Hyperpolarized (129) Xe Brain MR. *NMR Biomed.* **2016**, *29* (3), 220−225.
(6) Stevens, T. K.; Ramirez, R. M.; Pines, A. Nanoemulsion Contrast Agents with Sub-Picomolar Sensitivity for Xenon NMR. *J. Am. Chem. Soc.* **2013**, *135* (26), 9576−9579.
(7) Riggle, B. A.; Wang, Y. F.; Dmochowski, I. J. A "Smart" Xe-129 NMR Biosensor for pH-Dependent Cell Labeling. *J. Am. Chem. Soc.* **2015**, *137* (16), 5542−5548.
(8) Bai, Y.; Hill, P. A.; Dmochowski, I. J. Utilizing a Water-Soluble Cryptophane with Fast Xenon Exchange Rates for Picomolar Sensitivity NMR Measurements. *Anal. Chem.* **2012**, *84* (22), 9935−9941.
(9) Schlundt, A.; Kilian, W.; Beyermann, M.; Sticht, J.; Gunther, S.; Hopner, S.; Falk, K.; Roetzschke, O.; Mitschang, L.; Freund, C. A Xenon-129 Biosensor for Monitoring MHC-Peptide Interactions. *Angew. Chem., Int. Ed.* **2009**, *48* (23), 4142−4145.
(10) Boutin, C.; Stopin, A.; Lenda, F.; Brotin, T.; Dutasta, J. P.; Jamin, N.; Sanson, A.; Boulard, Y.; Leteurtre, F.; Huber, G.; Bogaert-Buchmann, A.; Tassali, N.; Desvaux, H.; Carriere, M.; Berthault, P. Cell Uptake of a Biosensor Detected by Hyperpolarized Xe-129 NMR: The Transferrin Case. *Bioorg. Med. Chem.* **2011**, *19* (13), 4135−4143.
(11) Kotera, N.; Dubost, E.; Milanole, G.; Doris, E.; Gravel, E.; Arhel, N.; Brotin, T.; Dutasta, J. P.; Cochrane, J.; Mari, E.; Boutin, C.; Leonce, E.; Berthault, P.; Rousseau, B. A Doubly Responsive Probe for the Detection of Cys4-Tagged Proteins. *Chem. Commun.* **2015**, *51* (57), 11482−11484.
(12) Wei, Q.; Seward, G. K.; Hill, P. A.; Patton, B.; Dimitrov, I. E.; Kuzma, N. N.; Dmochowski, I. J. Designing Xe-129 NMR Biosensors for Matrix Metalloproteinase Detection. *J. Am. Chem. Soc.* **2006**, *128* (40), 13274−13283.
(13) Chambers, J. M.; Hill, P. A.; Aaron, J. A.; Han, Z. H.; Christianson, D. W.; Kuzma, N. N.; Dmochowski, I. J. Cryptophane Xenon-129 Nuclear Magnetic Resonance Biosensors Targeting Human Carbonic Anhydrase. *J. Am. Chem. Soc.* **2009**, *131* (2), 563−569.
(14) Zhang, B.; Guo, Q.; Luo, Q.; Zhang, X.; Zeng, Q.; Zhao, L.; Yuan, Y.; Jiang, W.; Yang, Y.; Liu, M.; Ye, C.; Zhou, X. An Intracellular Diamine Oxidase Triggered Hyperpolarized Xe-129 Magnetic Resonance Biosensor. *Chem. Commun.* **2018**, *54* (97), 13654−13657.
(15) Roy, V.; Brotin, T.; Dutasta, J. P.; Charles, M. H.; Delair, T.; Mallet, F.; Huber, G.; Desvaux, H.; Boulard, Y.; Berthault, P. A Cryptophane Biosensor for the Detection of Specific Nucleotide Targets through Xenon NMR Spectroscopy. *ChemPhysChem* **2007**, *8* (14), 2082−2085.
(16) Khan, N. S.; Riggle, B. A.; Seward, G. K.; Bai, Y. B.; Dmochowski, I. J. Cryptophane-Folate Biosensor for Xe-129 NMR. *Bioconjugate Chem.* **2015**, *26* (1), 101−109.
(17) Palaniappan, K. K.; Ramirez, R. M.; Bajaj, V. S.; Wemmer, D. E.; Pines, A.; Francis, M. B. Molecular Imaging of Cancer Cells Using a Bacteriophage-Based ^{129}Xe NMR Biosensor. *Angew. Chem., Int. Ed.* **2013**, *52* (18), 4849−4853.
(18) Witte, C.; Martos, V.; Rose, H. M.; Reinke, S.; Klippel, S.; Schroder, L.; Hackenberger, C. P. R. Live-Cell MRI with Xenon Hyper-CEST Biosensors Targeted to Metabolically Labeled Cell-Surface Glycans. *Angew. Chem., Int. Ed.* **2015**, *54* (9), 2806−2810.
(19) Rose, H. M.; Witte, C.; Rossellaa, F.; Klippel, S.; Freund, C.; Schroder, L. Development of an Antibody-Based, Modular Biosensor for Xe-129 NMR Molecular Imaging of Cells at Nanomolar Concentrations. *Proc. Natl. Acad. Sci. U. S. A.* **2014**, *111* (32), 11697−11702.
(20) Yang, S.; Jiang, W.; Ren, L.; Yuan, Y.; Zhang, B.; Luo, Q.; Guo, Q.; Bouchard, L. S.; Liu, M.; Zhou, X. Biothiol Xenon MRI Sensor Based on Thiol-Addition Reaction. *Anal. Chem.* **2016**, *88* (11), 5835−5840.
(21) Zeng, Q.; Guo, Q.; Yuan, Y.; Yang, Y.; Zhang, B.; Ren, L.; Zhang, X.; Luo, Q.; Liu, M.; Bouchard, L. S.; Zhou, X. Mitochondria Targeted and Intracellular Biothiol Triggered Hyperpolarized Xe-129 Magnetofluorescent Biosensor. *Anal. Chem.* **2017**, *89* (4), 2288−2295.
(22) Zemerov, S. D.; Roose, B. W.; Farenhem, K. L.; Zhao, Z.; Stringer, M. A.; Goldman, A. R.; Speicher, D. W.; Dmochowski, I. J. Xe-129 NMR-Protein Sensor Reveals Cellular Ribose Concentration. *Anal. Chem.* **2020**, *92* (19), 12817−12824.
(23) Roose, B. W.; Zemerov, S. D.; Dmochowski, I. J. Nanomolar Small-Molecule Detection Using a Genetically Encoded Xe-129 NMR Contrast Agent. *Chem. Sci.* **2017**, *8* (11), 7631−7636.
(24) Yang, S.; Yuan, Y.; Jiang, W.; Ren, L.; Deng, H.; Bouchard, L. S.; Zhou, X.; Liu, M. Hyperpolarized (129) Xe Magnetic Resonance Imaging Sensor for H_2S. *Chem. - Eur. J.* **2017**, *23* (32), 7648−7652.
(25) Berthault, P.; Desvaux, H.; Wendlinger, T.; Gyejacquot, M.; Stopin, A.; Brotin, T.; Dutasta, J. P.; Boulard, Y. Effect of pH and Counterions on the Encapsulation Properties of Xenon in Water-Soluble Cryptophanes. *Chem. - Eur. J.* **2010**, *16* (43), 12941−12946.
(26) Schilling, F.; Schroder, L.; Palaniappan, K. K.; Zapf, S.; Wemmer, D. E.; Pines, A. MRI Thermometry Based on Encapsulated Hyperpolarized Xenon. *ChemPhysChem* **2010**, *11* (16), 3529−3533.
(27) Zhang, L.; Burant, A.; McCallister, A.; Zhao, V.; Koshlap, K. M.; Degan, S.; Antonacci, M.; Branca, R. T. Accurate MR Thermometry by Hyperpolarized Xe-129. *Magn. Reson. Med.* **2017**, *78* (3), 1070−1079.
(28) Schroeder, L.; Meldrum, T.; Smith, M.; Lowery, T. J.; Wemmer, D. E.; Pines, A. Temperature Response of (129)Xe Depolarization Transfer and Its Application for Ultrasensitive NMR Detection. *Phys. Rev. Lett.* **2008**, *100* (25), 257603.
(29) Kotera, N.; Tassali, N.; Leonce, E.; Boutin, C.; Berthault, P.; Brotin, T.; Dutasta, J. P.; Delacour, L.; Traore, T.; Buisson, D. A.; Taran, F.; Coudert, S.; Rousseau, B. A Sensitive Zinc-Activated ^{129}Xe MRI Probe. *Angew. Chem., Int. Ed.* **2012**, *51* (17), 4100−4103.
(30) Zhang, J.; Jiang, W.; Luo, Q.; Zhang, X.; Guo, Q.; Liu, M.; Zhou, X. Rational Design of Hyperpolarized Xenon NMR Molecular Sensor for the Selective and Sensitive Determination of Zinc Ions. *Talanta* **2014**, *122*, 101−105.
(31) Guo, Q.; Zeng, Q.; Jiang, W.; Zhang, X.; Luo, Q.; Zhang, X.; Bouchard, L. S.; Liu, M.; Zhou, X. A Molecular Imaging Approach to Mercury Sensing Based on Hyperpolarized Xe-129 Molecular Clamp Probe. *Chem. - Eur. J.* **2016**, *22* (12), 3967−3970.
(32) Tassali, N.; Kotera, N.; Boutin, C.; Leonce, E.; Boulard, Y.; Rousseau, B.; Dubost, E.; Taran, F.; Brotin, T.; Dutasta, J. P.; Berthauet, P. Smart Detection of Toxic Metal Ions, Pb^{2+} and Cd^{2+}, Using a Xe-129 NMR-Based Sensor. *Anal. Chem.* **2014**, *86* (3), 1783−1788.
(33) Spence, M. M.; Rubin, S. M.; Dimitrov, I. E.; Ruiz, E. J.; Wemmer, D. E.; Pines, A.; Yao, S. Q.; Tian, F.; Schultz, P. G. Functionalized Xenon as a Biosensor. *Proc. Natl. Acad. Sci. U. S. A.* **2001**, *98* (19), 10654−10657.
(34) Schnurr, M.; Sloniec-Myszk, J.; Dopfert, J.; Schröder, L.; Hennig, A. Supramolecular Assays for Mapping Enzyme Activity by Displacement-Triggered Change in Hyperpolarized Xe-129 Magnetization Transfer NMR Spectroscopy. *Angew. Chem., Int. Ed.* **2015**, *54* (45), 13444−13447.
(35) Zaiss, M.; Schnurr, M.; Bachert, P. Analytical Solution for the Depolarization of Hyperpolarized Nuclei by Chemical Exchange Saturation Transfer between Free and Encapsulated Xenon (HyperCEST). *J. Chem. Phys.* **2012**, *136* (14), 144106.
(36) Korchak, S.; Kilian, W.; Mitschang, L. Degeneracy in Cryptophane-Xenon Complex Formation in Aqueous Solution. *Chem. Commun.* **2015**, *51* (9), 1721−1724.

https://doi.org/10.1021/acs.jpclett.1c02239
J. Phys. Chem. Lett. 2021, 12, 8652−8657

(37) Kunth, M.; Witte, C.; Schröder, L. Quantitative Chemical Exchange Saturation Transfer with Hyperpolarized Nuclei (qHyper-CEST): Sensing Xenon-Host Exchange Dynamics and Binding Affinities by NMR. *J. Chem. Phys.* **2014**, *141* (19), 194202.
(38) Korchak, S.; Kilian, W.; Schröder, L.; Mitschang, L. Design and Comparison of Exchange Spectroscopy Approaches to Cryptophane-Xenon Host-Guest Kinetics. *J. Magn. Reson.* **2016**, *265*, 139−145.
(39) Yuan, Y.; Guo, Q.; Zhang, X.; Jiang, W.; Ye, C.; Zhou, X. Silica Nanoparticle Coated Perfluorooctyl Bromide for Ultrasensitive MRI. *J. Mater. Chem. B* **2020**, *8* (23), 5014−5018.
(40) Kunth, M.; Witte, C.; Hennig, A.; Schröder, L. Identification, Classification, and Signal Amplification Capabilities of High-Turnover Gas Binding Hosts in Ultra-Sensitive NMR. *Chem. Sci.* **2015**, *6* (11), 6069−6075.
(41) Kunth, M.; Witte, C.; Schroder, L. Mapping of Absolute Host Concentration and Exchange Kinetics of Xenon Hyper-CEST MRI Agents. *Pharmaceuticals* **2021**, *14* (2), 79.
(42) Korchak, S.; Riemer, T.; Kilian, W.; Mitschang, L. Quantitative Biosensor Detection by Chemically Exchanging Hyperpolarized Xe-129. *Phys. Chem. Chem. Phys.* **2018**, *20* (3), 1800−1808.
(43) Boutin, C.; Leonce, E.; Brotin, T.; Jerschow, A.; Berthault, P. Ultrafast Z-Spectroscopy for (129)Xe NMR-Based Sensors. *J. Phys. Chem. Lett.* **2013**, *4* (23), 4172−4176.
(44) Dopfert, J.; Schnurr, M.; Kunth, M.; Rose, H. M.; Hennig, A.; Schroder, L. Time-Resolved Monitoring of Enzyme Activity with Ultrafast Hyper-CEST Spectroscopy. *Magn. Reson. Chem.* **2018**, *56* (7), 679−688.
(45) Xiao, G.; Sun, P. Z.; Wu, R. Fast Simulation and Optimization of Pulse-Train Chemical Exchange Saturation Transfer (CEST) Imaging. *Phys. Med. Biol.* **2015**, *60* (12), 4719−4730.
(46) Tyagi, R.; Witte, C.; Haag, R.; Schröder, L. Dendronized Cryptophanes as Water-Soluble Xenon Hosts for Xe-129 Magnetic Resonance Imaging. *Org. Lett.* **2014**, *16* (17), 4436−4439.
(47) Zemerov, S. D.; Roose, B. W.; Greenberg, M. L.; Wang, Y.; Dmochowski, I. J. Cryptophane Nanoscale Assemblies Expand Xe-129 NMR Biosensing. *Anal. Chem.* **2018**, *90* (12), 7730−7738.
(48) Ryoo, D.; Xu, X.; Li, Y. G.; Tang, J. A.; Zhang, J.; van Zijl, P. C. M.; Liu, G. S. Detection and Quantification of Hydrogen Peroxide in Aqueous Solutions Using Chemical Exchange Saturation Transfer. *Anal. Chem.* **2017**, *89* (14), 7758−7764.
(49) Zhou, X.; Graziani, D.; Pines, A. Hyperpolarized Xenon NMR and MRI Signal Amplification by Gas Extraction. *Proc. Natl. Acad. Sci. U. S. A.* **2009**, *106* (40), 16903−16906.
(50) Zeng, Q.; Bie, B.; Guo, Q.; Yuan, Y.; Han, Q.; Han, X.; Chen, M.; Zhang, X.; Yang, Y.; Liu, M.; Liu, P.; Deng, H.; Zhou, X. Hyperpolarized Xe NMR Signal Advancement by Metal-Organic Framework Entrapment in Solution. *Proc. Natl. Acad. Sci. U. S. A.* **2020**, *117* (30), 17558−17563.

https://doi.org/10.1021/acs.jpclett.1c02239
J. Phys. Chem. Lett. 2021, 12, 8652−8657